DOI 10.1007/s10946-024-10190-w
Journal of Russian Laser Research, Volume 45, Number 1, January, 2024

RESEARCH ON A BROADBAND COMPACT POLARIZATION BEAM SPLITTER

Zhibin Wang, Xuwei Hou,* Zhengyang Li, and Jiutian Zhang

School of Electrical Engineering, Yanshan University
Qinhuangdao, China

*Corresponding author e-mail: 964891317@qq.com

Abstract

Many devices based on silicon and other photonic integrated circuit platforms exhibit significant polarization dependence. Polarization beam splitter (PBS) is a device that split optical signals into transverse electric (TE) and transverse magnetic (TM) modes. Among various PBSs, asymmetric directional couplers are widely used due to their fine performance, but their working bandwidth is limited due to wavelength changes that can lead to deviations in effective refractive index and coupling strength. We propose a PBS, which uses metamaterial anisotropy to replace structural asymmetry and break the bandwidth bottleneck. It achieves good performance in the wavelength range of 258 nm, where the extinction ratio of the TM polarization is greater than 24 dB and that of the TE polarization is greater than 26 dB. It covers the E, S, C, L, and U bands, and the coupling area is as small as 7.25×2.625 μm, with a total device footprint of 15.65×6.125 μm.

Keywords: polarization beam splitter, metamaterial anisotropy, bandwidth.

1. Introduction

PBS is an important component of polarization diversity circuit, which can effectively separate TE and TM modes. Common types of PBS include Mach–Zehnder interferometer (MZI) [1,2], directional coupler (DC) [3,4], multi-mode interferometer (MMI) [5], grating assisted device [6], reverse design structure [7], sub-wavelength grating (SWG) [8] structures, etc. These traditional PBSs have a characteristic that, only when the phase matching condition is met and the coupling length is optimum, PBS can achieve complete coupling. The effective refractive index and coupling length vary with wavelength, so only at the central wavelength complete coupling can be ensured, resulting in a smaller working bandwidth. In almost all reports, the working bandwidth of PBS is smaller than 100 nm. By cascading multiple coupling segments, the working bandwidth can be increased to over 100 nm, but additional losses are also introduced [9].

Metamaterials [10] provide a new method for manipulating the light response and controlling the light flow, which has attracted attention due to its low loss and ease of manufacturing. It has extensive applications in modulators [11], resonators [12], absorbers [13], couplers [14], and other fields. SWG is a necessary and effective structure for synthesizing metamaterials due to its strong anisotropy and flat dispersion.

In recent years, there were many reports using anisotropic all dielectric metamaterials to improve performance indicators of silicon PBS. J. Zhang et al. proposed a super-compact and efficient polarization beam splitter, with a high polarization extinction ratio, based on photonic anisotropic metamaterials [15].

Manuscript submitted by the authors in English on December 27, 2023.

The coupling region of PBS is composed of two parallel metamaterial waveguides, which achieve extinction ratios of TE and TM modes of 46 and 33 dB, respectively, at a wavelength of 1550 nm, but the operating bandwidth is only 80 nm. A. Debevc et al. utilized the characteristics of all dielectric metamaterial cladding to increase the operating bandwidth to 140 nm [16]. Afterwards, an improved method was proposed to combine TE polarizers with MZI and metamaterials, successfully increasing the operating bandwidth to 263 nm. The extinction ratio of both modes is greater than 30 dB, but it also increases the overall device size to 82 μm, making the device difficult to process. C. Deng et al. provided theoretical modeling and numerical simulation of a polarization beam splitter based on heterogeneous-anisotropic metamaterials on a Lithium niobate platform on an insulator [17]. They proved strong robustness of manufacturing errors, but the extinction ratio of TM was low, with a maximum value of only 30 dB, and the equipment occupied a space of 8×160 μm, still very large, with a working bandwidth of only 85 nm.

In this paper, we use SWG anisotropic metamaterials to design a low loss, high extinction ratio, large broadband, and small size PBS. The coupling region is formed by the combination of SWGs arranged in different directions. Since birefringence is provided by anisotropic metamaterials rather than asymmetric waveguides, the coupling region is designed to be geometrically symmetric. The purpose of introducing metamaterials before the output port is to eliminate residual TM polarization and increase the operating bandwidth of PBS.

2. Principle and Design

During the design process, FDTD software is used for simulation to construct a 3D model. Divide the grid into 10∼20 nm, the outer boundary of the solver is greater than 500 nm above and below the waveguide; see Fig. 1.

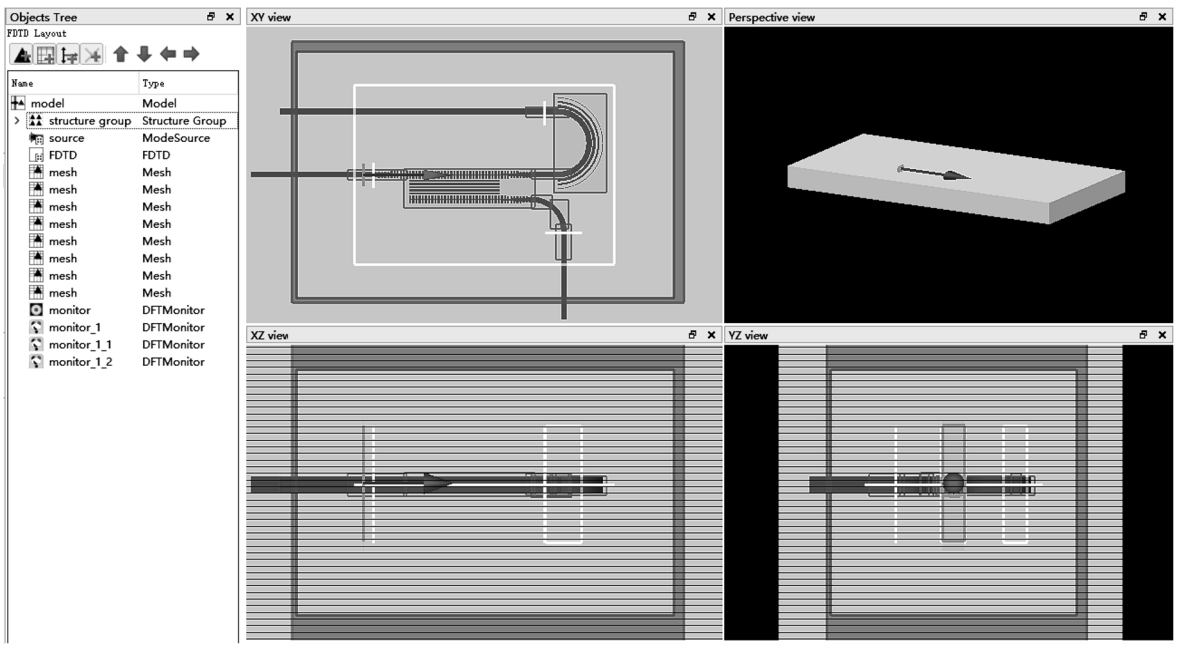

Fig. 1. Schematic diagram of the 3D model of PBS in FDTD.

The PBS is designed based on the SOI platform, with a height of Si of 250 nm and the entire device wrapped in SiO_2. The effective refractive index of SiO_2 is 1.445, and the effective refractive index of Si waveguide at the cross-section is 3.455. In Fig. 2, we show a schematic diagram of the PBS. The SWG anisotropic metamaterial parallel to the X and Y axes in coupling region A is represented by AM_1 and AM_2, while the SWG anisotropic metamaterial in region C is represented by AM_3; see Fig. 2 a. The effective refractive index of SWG anisotropy can be obtained, using the effective medium theory [18],

$$n_o = f \cdot n_{\mathrm{Si}}^2 + (1-f) \cdot n_{\mathrm{SiO_2}}^2, \tag{1}$$

$$\frac{1}{n_e^2} = \frac{f}{n_{\mathrm{Si}}^2} + \frac{1-f}{n_{\mathrm{SiO_2}}^2}, \tag{2}$$

where n_o and n_e are the refractive indices of ordinary light and extraordinary light, and f is the duty

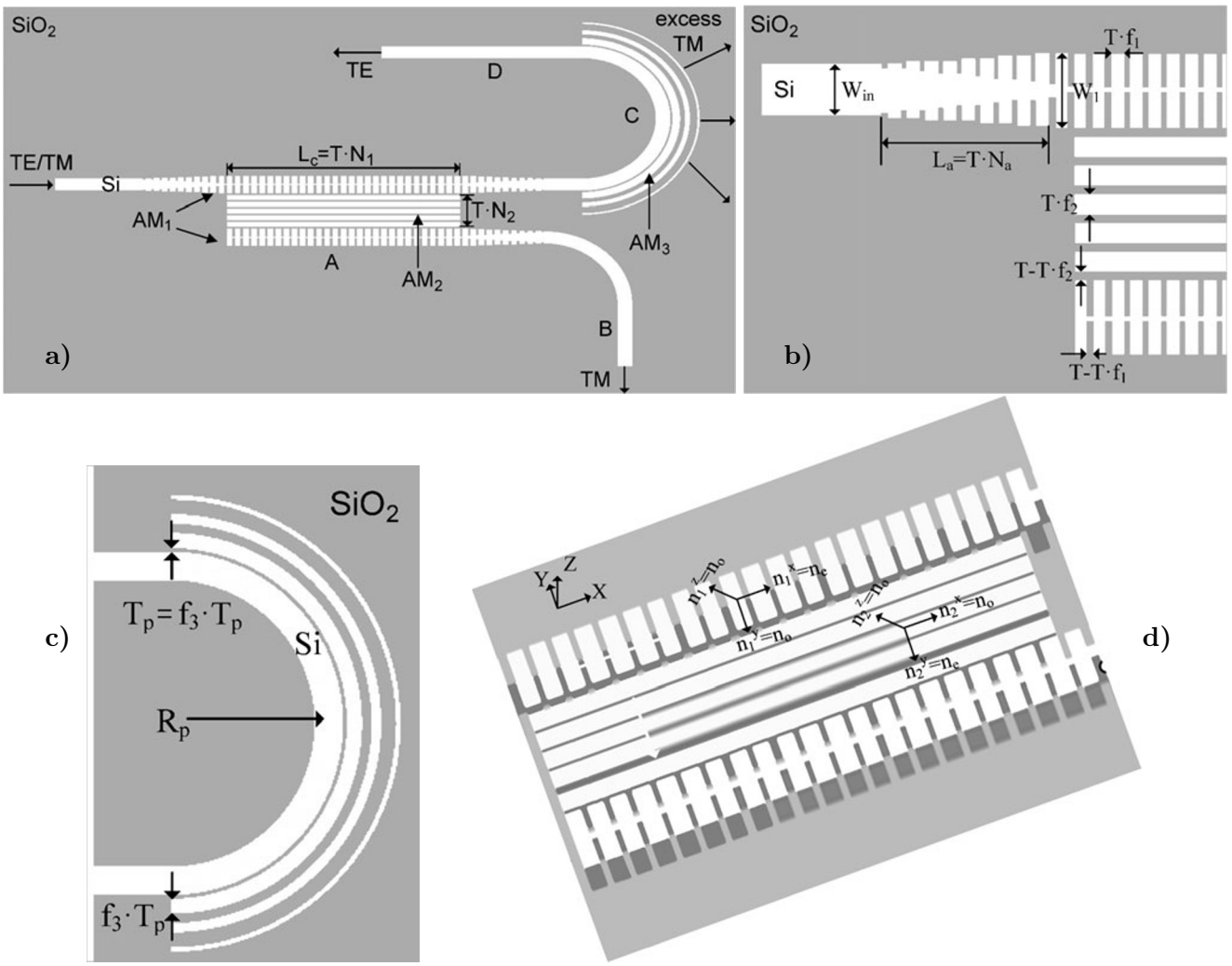

Fig. 2. Top view of polarization beam splitter (a), enlarged schematic diagram of the input port with some key parameters marked (b), enlarged schematic diagram of TE mode output port with some key parameters marked (c), enlarged schematic diagram of the coupling area, with yellow arrows indicating the direction of the optical axis and green and blue arrows indicating the direction of the TM and TE polarizations, respectively (d).

cycle of SWG. The diagonal effective refractive index tensors n_1 and n_2 of AM_1 and AM_2 are defined as

$$n_1 = \mathrm{diag}[n_1^x, n_1^y, n_1^z] = \mathrm{diag}[n_e, n_o, n_o], \tag{3}$$

$$n_2 = \mathrm{diag}[n_2^x, n_2^y, n_2^z] = \mathrm{diag}[n_o, n_e, n_o]. \tag{4}$$

One can see that the TM polarization with electrical components in the Z direction has an effective refractive index n_o in regions AM_1 and AM_2, which satisfies the phase matching condition and can effectively couple the TM-polarized light to the lower optical waveguide and output from port B. For the TE polarization with electrical components in the Y direction, the effective refractive indices of AM_1 and AM_2 are n_o and n_e, respectively, which do not meet the phase matching condition. The TE polarized light is output directly from port D without coupling; see Fig. 2 d.

The period of SWG is selected as $T = 250$ nm, the width of the input waveguide $W_{\mathrm{in}} = 450$ nm to ensure the single-mode propagation, and the width W_1 of AM_1 is 650 nm to reduce diffraction losses at the input and output ports. As shown in Fig. 2 b, a longitudinally arranged grating is introduced between the coupling region and the input port, with a width linearly increasing in steps of 20 nm and a cycle number of $N_a = 10$. Each grating is sequentially connected, and the width of Si connected to the grating is linearly reduced in steps of 30 nm to form a tapered waveguide. This ensures complete conversion of polarized light between the channel waveguide and SWG [19], while suppressing the diffraction and minimizing reflection loss. In coupling region A, the gratings within the region AM_1 are connected by Si with a width of 50 nm, making the hetero-anisotropic plate a uniformly distributed multimode interference coupler [20], the incident TM polarized light can effectively couple. As shown in Fig. 1 c, in region C, the radius of the curved waveguide is $R_p = 2.5$ μm, the period of the curved grating in region AM_3 is $T_p = 300$ nm, the duty cycle f_3 linearly changes from 0.8 to 0.2, and the number of cycles $N_3 = 3$. The designed structure couples the residual TM polarization into free space through AM_3, and the principle will be discussed in detail in other papers.

The duty cycle of AM_1 is f_1 with N_1 cycles, and the duty cycle of AM_2 is f_2 with N_2 cycles. Take $N_1 = 29$ and $N_2 = 5$ as the initial values. The duty cycle is taken as $f_1 = f_2 = f_0$, and FDTD is used for numerical optimization. The value of f_0 is scanned from 0.4 to 0.9, and a monitor is introduced in region B to calculate the power ratio of TM. The results are shown in Fig. 3. When $f_0 = 0.7$, the power ratio reaches a maximum value of 0.88.

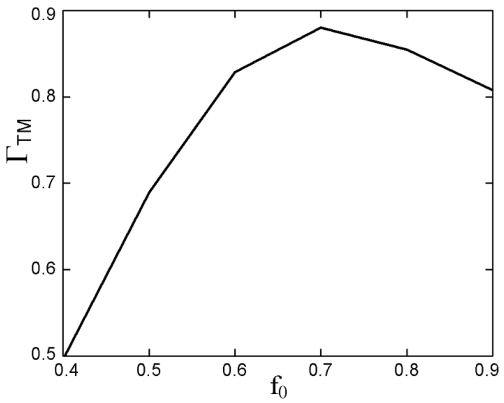

Fig. 3. The power ratio of the TM polarization as a function of f_0.

The indicators for evaluating the quality of PBS include not only transmittance but also extinction ratio (PER) and insertion loss (IL). They are defined as follows:

$$\mathrm{PER_{TM}} = 10\log_{10}\frac{P_{\mathrm{TM\_B}}}{P_{\mathrm{TM\_D}}}, \tag{5}$$

$$\mathrm{PER_{TE}} = 10\log_{10}\frac{P_{\mathrm{TM\_D}}}{P_{\mathrm{TM\_B}}}, \tag{6}$$

$$\mathrm{IL_{TM}} = 10\log_{10}\frac{P_{\mathrm{TM\_B}}}{P_{\mathrm{Input\_TM}}}, \tag{7}$$

$$\mathrm{IL_{TE}} = 10\log_{10}\frac{P_{\mathrm{TE\_D}}}{P_{\mathrm{Input\_TE}}}. \tag{8}$$

In these formulas, $P_{\mathrm{TM\_B}}$, $P_{\mathrm{TM\_D}}$, $P_{\mathrm{TE\_B}}$, and $P_{\mathrm{TE\_D}}$ are the powers of the TM and TE polarizations at

output ports B and D, and $P_{\text{Input\_TE}}$ and $P_{\text{Input\_TE}}$ represent the power of the TM and TE polarizations at the input port.

Due to the significant impact of AM_1 arrangement on the coupling effect of the TM polarization, we fix the value of f_2 at 0.7, and further optimized f_1 from 0.6 to 0.8 in steps of 0.02. While calculating transmittance, we also calculate PER and IL. In Fig. 4 a, one can see that, when f_1 is between 0.64 and 0.74, the transmittances of the TE and TM polarizations are larger than 81% for both. As shown in Fig. 4 b and c, within the same value range of f_1, the PER of the two polarizations is larger than 2 dB, and the IL is smaller than 0.9 dB. Especially at $f_1 = 0.7$, the PER of TM polarization reaches its maximum value equal to 34 dB and IL is 0.55 dB, while the PER of TE polarization is equal to 28 dB and IL is 0.7 dB. Based on the simulation results of these parameters, we ultimately take the duty cycle f_1 to be equal to 0.7.

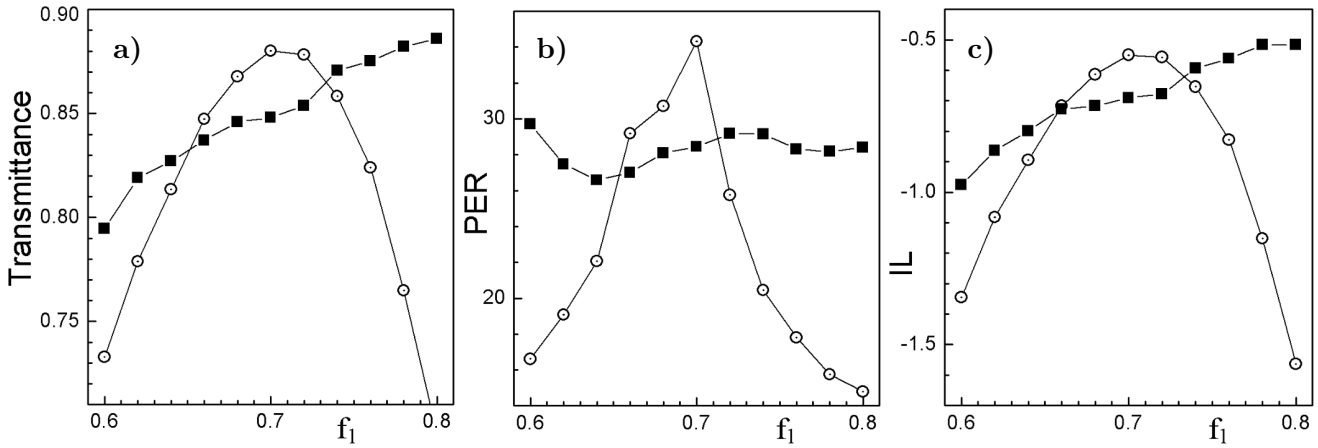

Fig. 4. The variation of transmittance (a), PER (b), and IL (c) with f_1 for the TE polarization (■) and for the TM polarization (⊙).

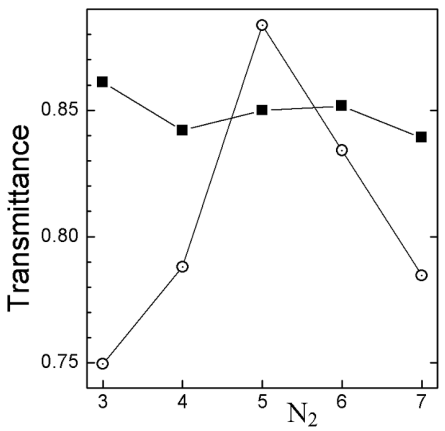

Fig. 5. Changes in transmittance with N_2.

By analyzing the transmittances of the TE and TM polarizations under different values, we can select an appropriate number of cycles N_2. In Fig. 5, we see that, when the TE and TM polarized light is the output from ports D and B, the transmittance of the TE polarization does not significantly change with N_2, maintaining fluctuations of around 84% to 86%. The transmittance of the TM polarization reaches 89% when $N_2 = 5$.

The calculation formula for coupling length reads

$$L_c = \frac{\lambda}{2(n_{\text{odd}} - n_{\text{even}})}, \tag{9}$$

where L_c is the coupling length, n_{odd} and n_{even} are the effective refractive indices of odd and even symmetric modes, and λ is the wavelength of the incident light. The wavelength is selected as $\lambda =$ 1550 nm, and the MODE software is used to calculate the n_{odd} and n_{even} of the TM polarization at $f_1 = 0.7$, $N_2 = 5$, and $f_2 = 0.7$; they are 1.949 and 1.843, respectively. Substituting them into formula (9), we obtain the L_c of the TM polarization equal to 7.3 μm. The n_{odd} and n_{even} of the TE polarization

are 2.4782 and 2.4778, respectively, and the L_c of the TE polarization obtained by substitution is 1937.5 μm. The coupling length difference between the TM polarization and the TE polarization is several orders of magnitude, thus achieving the TM polarization coupling while suppressing the TE polarization coupling.

Different λ correspond to different L_c, so the coupling length of TM fluctuates around 7.3 μm with the change of wavelength. When $L_c = 7.3$ μm, the number of cycles N_1 of AM_1 is about 29. By linearly changing N_1 from 20 to 34, we obtain the transmittance, PER, and IL of the TE and TM polarizations passing through regions D and B; see Fig. 5. After analysis, L_c is corrected to the optimum coupling length. In Fig. 6 b, when $N_1 = 27$, the PER of TE polarization reaches the maximum value equal to 37 dB. However, in Fig. 6 a and c, the transmittance and insertion loss of TM do not achieve the desired effect. Considering the overall performance of the device, $N_1 = 29$ is chosen.

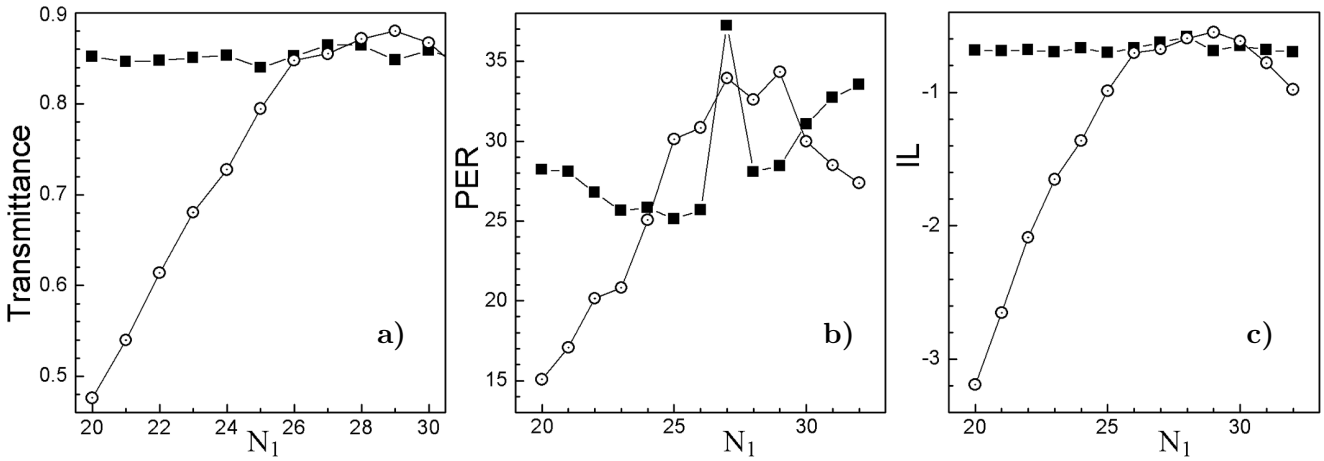

Fig. 6. The variation of transmittance (a), PER (b), and IL (c) with N_1 for the TE polarization (■) and for the TM polarization (⊙).

Table 1. Optimization of PBS Parameters.

AM_1	$T = 250$ nm	$N_1 = 29$	$f_1 = 0.7$	$L_c = 7.25$ μm
	$L_a = 2.5$ μm	$N_a = 10$	$W_1 = 650$ nm	$W_{\text{in}} = 450$ nm
AM_2	$T_P = 300$ nm	$N_3 = 3$	$R_P = 2.5$ μm	
	$T = 250$ nm	$N_2 = 5$	$f_2 = 0.7$	

In Table 1, we present the optimized parameters of the designed PBS.

Based on the optimized parameters, we simulate the optical field transmission of the TM and TE polarizations in PBS within the coupling region A; see Fig. 7. One can see that the TM polarized light is effectively coupled to the lower waveguide and output from port B. The TE polarized light propagates along a straight line and outputs from port D, separating the TE polarized light from the TM polarized light.

The manufacturing process of the device is as follows;

- On the SOI platform, a layer of SiO_2 cladding with a thickness of 400 nm is prepared, using appropriate methods.

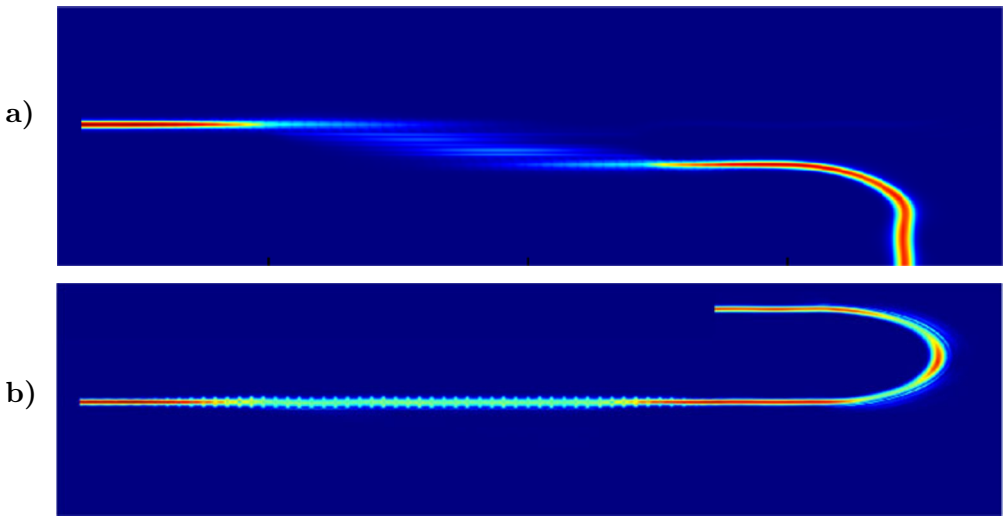

Fig. 7. Optical field transmission of the TM polarization (a) and the TE polarization (b) in PBS.

- Using photolithography technology, a grating structure with a certain period is prepared on the cladding surface to meet the optical performance requirements of polarization for beam splitters.
- Using ion implantation doping technology, doping agents are injected into the grating region to change its refractive index, thereby forming a waveguide structure.
- Plasma etching is performed on the waveguide structure to remove unwanted silicon materials and form the basic structure of PBS.
- Clean the etched PBS and perform photolithography again to achieve higher precision and more complex optical structures.

The above is a brief overview of the processing and manufacturing steps of SiO_2 cladding PBS based on the SOI platform. The specific operational details and parameter settings still need to be adjusted and optimized according to the specific equipment, process, and experimental conditions.

3. Performance Analysis of the Device

In Fig. 8, we show the PER and IL of the TE and TM polarizations at different wavelengths. The smaller the IL of the polarization beam splitter, the higher the performance of the device, and the maximum cannot exceed 2 dB, otherwise it will seriously affect the coupling of the TM mode. During the manufacturing process of devices, there may inevitably be some size errors. In order to ensure good performance of the device, selecting an IL smaller than 1.35 dB increases the manufacturing tolerance of the device. In the wavelength range of 1412 – 1670 nm, the PER of TM polarization is larger than 24 dB, and the IL is smaller than 1.35 dB. At a center wavelength of 1550 nm, the PER is 34 dB, and the IL is 0.55 dB. The TE polarization has a PER larger than 26 dB and IL smaller than 0.9 dB, with PER = 28 dB and IL = 0.7 dB at a center wavelength of 1550 nm. The PBS achieves a large operating bandwidth of 258 nm with relatively excellent parameter performance; it covers the E, S, C, L, and U bands of light.

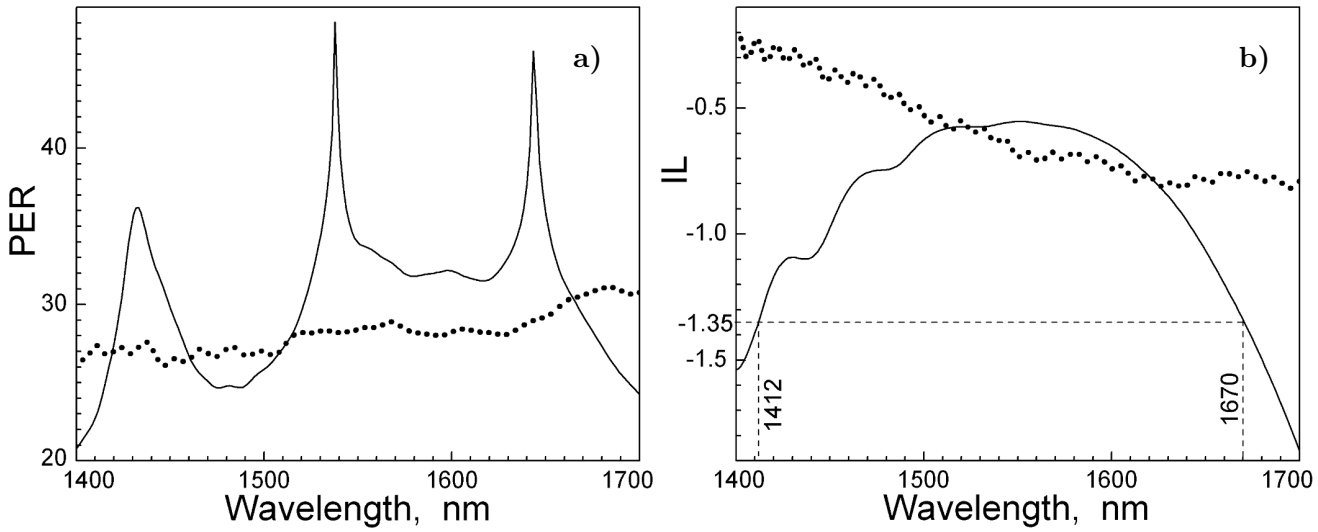

Fig. 8. Changes of PER and IL with wavelength for the TE polarization (dotted curves) and for the TM polarization (solid curves).

The process tolerance is selected to be evaluated within the range of ± 20 nm waveguide width variation and ±5 nm waveguide thickness variation. The waveguide width error ΔW ($W_{\text{in}} = W_{\text{in}} + \Delta W$) of PBS varies from − 20 nm to + 20 nm with equal intervals of 10 nm, and the Si waveguide thickness error Δh ($h = h + \Delta h$) of PBS varies from − 5 to + 5 nm, with equal intervals of 5 nm. In order to make the image clearer and more intuitive, PER is taken as a negative number. In Fig. 9, we show the variation of PER and IL with different waveguide width and thickness deviations for the TE and TM polarization input in the designed PBS. It can be seen that, when the waveguide width and thickness are far from the initial values, each curve exhibits different fluctuations. As shown in Fig. 9 a, b, within the tolerance range of ±20 nm waveguide width, when the TE polarization is input, the IL is smaller than 0.9 dB, and the PER is smaller than −24 dB. When inputting the TM polarization, the IL is smaller than 1.5 dB and PER is smaller than −24.5 dB. As shown in Fig. 9 c, d, within the tolerance range of ±5 nm Si waveguide thickness, the ILs of both polarizations are smaller than 1.8 dB, and the PERs are smaller than −19 dB. According to simulation analysis, the device has a considerable manufacturing tolerance, and within the tolerance range, the performance of the device is good.

Table 2. Performance Comparison between the Proposed PBS and Other PBSs with Different Structures.

Reference	PER, dB	IL, dB	Band width, nm	Coupling length, μm
Structure 1	> 25	< 0.7	175	11
Structure 2	> 23.07	< 0.93	85	19
Structure 3	> 26.1	< 0.27	200	32
Structure 4	> 28.15	< 0.66	210	12
Structure 5	> 15.4	< 2.72	40	12
This work	> 24	< 1.35	258	7.25

In Table 2, we present the comparison between the important parameters of the PBS designed here and those in recent papers. Structure 1 is a PBS consisting of two two-stage etched asymmetric directional

couplers designed by Y. Huang et al. [21], Structure 2 is a silicon nano-bridge waveguide assisted PBS designed by H. Liu et al. [22], Structure 3 is a PBS based on an x-cut Lithium niobate insulator platform designed by X. Li et al. [23], Structure 4 is a PBS based on Lithium niobate thin film asymmetric directional coupler designed by F. Wang et al. [24], Structure 5 is a PBS based on a silicon-on-insulator platform designed by M. A. Butt et al. [25]. In Table 2, we can see that, compared with the reported PBSs, the PBS proposed in this paper has good performance and achieves a large working bandwidth of 258 nm.

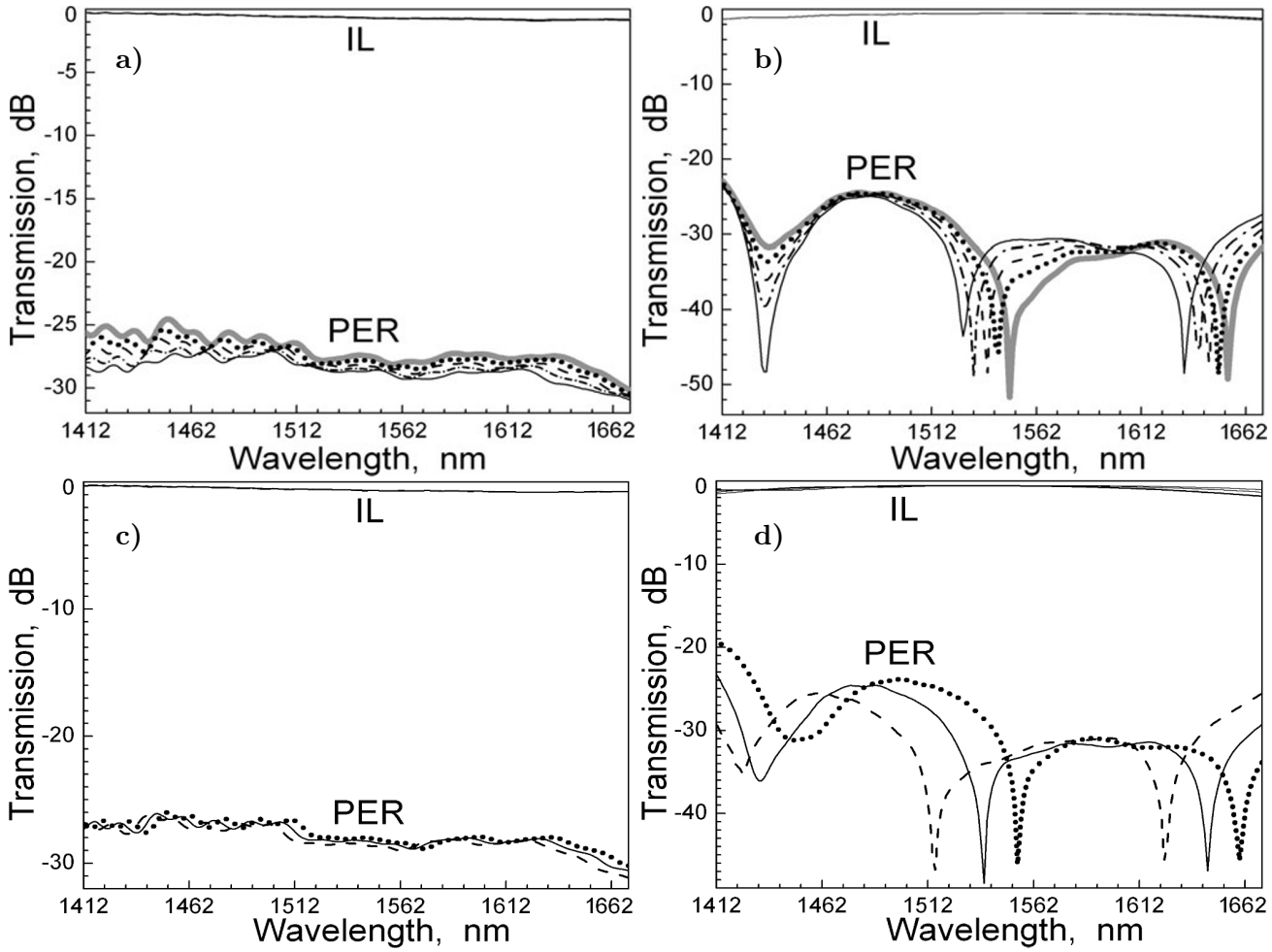

Fig. 9. Effect of the waveguide width manufacturing tolerance on the TE polarization (a) and the TM polarization (b), here $\Delta W = -20$ nm (solid curves), $\Delta W = -10$ nm (dash-dotted curves), $\Delta W = 0$ (dashed curves), $\Delta W = 10$ nm (dotted curves), and $\Delta W = 20$ nm (gray curves). Effect of waveguide height manufacturing tolerance on the TE polarization (c) and the TM polarization (d), here $\Delta h = -5$ nm (dashed curves), $\Delta h = 0$ (solid curves), and $\Delta h = 5$ nm (dotted curves).

4. Conclusions

In this paper, we proposed a silicon on chip PBS, using effective anisotropic metamaterials, which utilizes SWGs with different orientations to construct heterogeneous anisotropic plates, achieving the

TM polarization coupling, and suppressing the TE polarization coupling. This new structure can provide significant birefringence without disrupting geometric symmetry, while the metamaterial structure introduced in region C functions as a TE polarizer, which helps to increase the bandwidth. The device only uses Si and SiO_2 materials, combining rectangular and curved waveguides. It has a simple structure and is easy to manufacture, while achieving good performance, such as low loss, high extinction ratio, large working bandwidth, and small footprint. The simulation results show that, within the wavelength range of 1412 – 1670 nm, the device outputs for the TM polarization with PER $>$ 24 dB and IL $<$ 1.35 dB, and the TE polarization with PER $>$ 26 dB and IL $<$ 0.9 dB, achieving a working bandwidth of 258 nm at low loss. The proposed design method is also feasible, and PBSs can be implemented on SOIs of different thicknesses or even other platforms. This PBS has potential applications in silicon photonic integrated circuits, providing technical support for the next generation of optical communication.

Acknowledgments

This work was supported in part by the S&T Program of Hebei under Grants Nos. 206Z1703G and 62275228, the Key Research and Development Project of Hebei Province, China under Grants Nos. 19273901D and 20373301D, and the Natural Science Foundation of Hebei Province, China under Grant No. F2020203066.

References

1. J. Wang, J. Hao, J. Zhou, et al., *Sens. Actuator A Phys.*, **359**, 114465 (2023).
2. M. Yang, Y. Yao, H. Zhang, et al., *Opt. Laser Technol.*, **163**, 109310 (2023).
3. A. Yadav, A. Kumar, and A. Prakash, *Optik*, **288**, 171190 (2023).
4. X. Nan, L. Dong, J. Dong, et al., *Opt. Laser Technol.*, **163**, 109413 (2023).
5. D. Hassan and D. Chack, *Microelectron. J.*, **104**, 104887 (2020).
6. Y. Zhao, Y. Shi, D. Liu, et al., *Opt. Commun.*, **550**, 130007 (2024).
7. Q. Lu, W. Wei, X. Yan, et al., *Photonics Nanostruct.*, **32**, 19 (2018).
8. M. A. Butt, C. Tyszkiewicz, K. Wojtasik, et al., *Int. J. Mol. Sci.*, **23**, 6614 (2022); DOI: 10.3390/ijms23126614
9. T. Huang, Y. Xie, Y. Wu, et al., *Appl. Opt.*, **58**, 2264 (2019).
10. N. L. Kazanskiy, S. N. Khonina, and M. A. Butt, *Nanomaterials*, **13**, 118 (2023); DOI: 10.3390/nano13010118
11. D. Wang, J. Tian, T. Ma, et al., *Opt. Commun.*, **23**, 130040 (2023).
12. W. Dong, T. Wang, Z. Huang, et al., *Thin-Wall. Struct.*, **191**, 110930 (2023).
13. N. Ullah, M. Islam, A. Hoque, et al., *Opt. Laser Technol.*, **168**, 109836 (2024).
14. E. Zayed, M. Alngar, A. Biswas, et al., *Optik*, **247**, 167960 (2021).
15. J. Zhang, X. Shi, Z. Zhang, et al., *Opt. Express*, **30**, 538 (2022).
16. A. Debevč, M. Topič, and M. Krč, *Opt. Express*, **30**, 46693 (2022); DOI: 10.1364/OE.476333
17. C. Deng, M. Lu, Y. Sun, et al., *Opt. Express*, **29**, 11627 (2021).
18. S. Zare, R. Pouria, and S. Edalatpour, *J. Quant. Spectrosc. Radiat. Transf.*, **216**, 107482 (2021).
19. J. Wang, I. Glesk, and L. Chen, *Sci. Bull.*, **61**, 879 (2016); DOI: 10.1007/s11434-016-1077-z
20. P. A. Besse, M. Bachmann, and H. Melchior, *J. Lightw. Technol.*, **12**, 1004 (1994).
21. Y. Huang, X. Zhou, C. Xie, et al., *Appl. Opt.*, **62**, 965 (2023).
22. H. Liu, J. Feng, J. Chen, et al., *Opt. Laser Technol.*, **167**, 109684 (2023).
23. X. Li, J. Tao, Y. Zhao, et al., *Opt. Commun,*, **545**, 129629 (2023).
24. F. Wang, H. Liu, T. Ma, et al., *Appl. Opt.*, **62**, 21 (2023).
25. M. A. Butt, S. N. Khonina, and N. L. Kazanskiy, *Laser Phys.*, **28**, 116202 (2018).